nature structural & molecular biology

ARTICLES

https://doi.org/10.1038/s41594-022-00814-7

Check for updates

OPEN

A conformational switch controlling the toxicity of the prion protein

Karl Frontzek[1,9], Marco Bardelli[2,3,9], Assunta Senatore[1,9], Anna Henzi[1], Regina R. Reimann[1], Seden Bedir[1], Marika Marino[4], Rohanah Hussain[5], Simon Jurt[6], Georg Meisl[7], Mattia Pedotti[2], Federica Mazzola[2], Giuliano Siligardi[5], Oliver Zerbe[6], Marco Losa[1], Tuomas Knowles[7], Asvin Lakkaraju[1], Caihong Zhu[1], Petra Schwarz[1], Simone Hornemann[1], Matthew G. Holt[4,8], Luca Simonelli[2], Luca Varani[2,10] ✉ and Adriano Aguzzi[1,10] ✉

Prion infections cause conformational changes of the cellular prion protein (PrP^{C}) and lead to progressive neurological impairment. Here we show that toxic, prion-mimetic ligands induce an intramolecular R208-H140 hydrogen bond ('H-latch'), altering the flexibility of the α2–α3 and β2–α2 loops of PrP^{C}. Expression of a PrP^{2Cys} mutant mimicking the H-latch was constitutively toxic, whereas a PrP^{R207A} mutant unable to form the H-latch conferred resistance to prion infection. High-affinity ligands that prevented H-latch induction repressed prion-related neurodegeneration in organotypic cerebellar cultures. We then selected phage-displayed ligands binding wild-type PrP^{C}, but not PrP^{2Cys}. These binders depopulated H-latched conformers and conferred protection against prion toxicity. Finally, brain-specific expression of an antibody rationally designed to prevent H-latch formation prolonged the life of prion-infected mice despite unhampered prion propagation, confirming that the H-latch is an important reporter of prion neurotoxicity.

The neurotoxicity of prions requires the interaction of the misfolded prion protein PrP^{Sc} with its cellular counterpart PrP^{C} (ref. [1]), which ultimately leads to depletion of the PIKfyve kinase[2] and to spongiform encephalopathy. Prion toxicity is initiated by unknown mechanisms that require membrane-bound PrP^{C} (refs. [1,3]). PrP^{C} is a glycosylphosphaidylinositol (GPI)-anchored protein composed of an amino-terminal, unstructured 'flexible tail' (FT) and a carboxy-terminal, structured 'globular domain' (GD)[4]. Mice lacking the prion protein gene *Prnp* do not succumb to prion diseases[5]. Antibodies binding the globular domain (GD) of PrP^{C} can halt this process[6], but they can also activate toxic intracellular cascades[7–9]. Similar events occur in prion-infected brains, and substances that counteract the damage of infectious prions can also alleviate the toxicity of anti-PrP^{C} antibodies, such as POM1 (ref. [8]). POM1 exerts its toxicity without inducing the formation of infectious prions[10], arguing that toxicity is independent of prion replication. Accordingly, toxicity can be very effectively prevented by the therapeutic co-stabilization of FT and GD through bispecific antibodies[11]. These findings suggest that POM1 and prions exert their toxicity through similar mechanisms.

To explore the causal links between the binding of POM1 to PrP^{C} and its neurotoxic consequences, we performed structural and molecular studies in silico, in vitro and in vivo. We found that the induction of an intramolecular hydrogen bond between R208 and H140 of the globular domain of human PrP^{C} ($hPrP^{C}$) is an early molecular reporter of prion toxicity.

Results

POM1 introduces an intramolecular hydrogen bond in PrP^{C}-GD. Structural analysis and molecular dynamics (MD) simulations indicated that POM1 induces an intramolecular hydrogen bond in both human and murine PrP^{C} between R208 and H139 in murine PrP^{C} (ref. [12]). This 'H-latch' constrains the POM1 epitope while allosterically increasing the flexibility of the β2–α2 and α2–α3 loops (Fig. 1 and Extended Data Fig. 1). To explore its role in prion toxicity, we generated a murine PrP^{R207A} mutant that prevents the H-latch without altering the conformation of PrP (Extended Data Fig. 1). We stably expressed murine PrP^{R207A} ($mPrP^{R207A}$) in $Prnp^{-/-}$ CAD5 cells[13] and $Prnp^{ZH3/ZH3}$ cerebellar organotypic cultured slices (COCS; Fig. 2a–c and Extended Data Fig. 2a–c)[14,15]. A panel of conformation-specific anti-PrP antibodies showed similar staining patterns for PrP^{C} and $mPrP^{R207A}$, confirming that both proteins folded properly but had reduced POM1 binding (Extended Data Fig. 2d,e), as expected from the structure of PrP–POM1 co-crystals[12]. $Prnp^{-/-}$ CAD5 cells expressing $mPrP^{R207A}$ were resistant to POM1 toxicity and, notably, showed impaired prion replication (Fig. 2d–f), pointing to common toxic properties.

Lack of the H-latch confers resistance to prion and POM1 toxicity. To test whether its presence can induce toxicity even in the absence of ligands, we designed an R207C-I138C double-cysteine PrP^{C} mutant (PrP^{2Cys} Fig. 3a,b), with the goal of replicating the structural effects of the H-latch in the absence of POM1 binding. Nuclear magnetic resonance (NMR) and MD analysis of recombinant $mPrP^{2Cys}$ were consistent with a folded protein resembling the

[1]Institute of Neuropathology, University of Zurich, Zurich, Switzerland. [2]Institute for Research in Biomedicine, Università della Svizzera italiana, Bellinzona, Switzerland. [3]PetMedix Ltd, Babraham Research Campus, Cambridge, UK. [4]Laboratory of Glia Biology, VIB-KU Leuven Center for Brain and Disease Research, Leuven, Belgium. [5]B23 Beamline, Diamond Light Source, Harwell Science Innovation Campus, Didcot, UK. [6]University of Zurich, Department of Chemistry, Zurich, Switzerland. [7]Department of Chemistry, University of Cambridge, Cambridge, UK. [8]Laboratory of Synapse Biology, Instituto de Investigação e Inovação em Saúde (i3S), University of Porto, Porto, Portugal. [9]These authors contributed equally: Karl Frontzek, Marco Bardelli, Assunta Senatore. [10]These authors contributed equally: Luca Varani, Adriano Aguzzi. ✉e-mail: luca.varani@irb.usi.ch; adriano.aguzzi@usz.ch

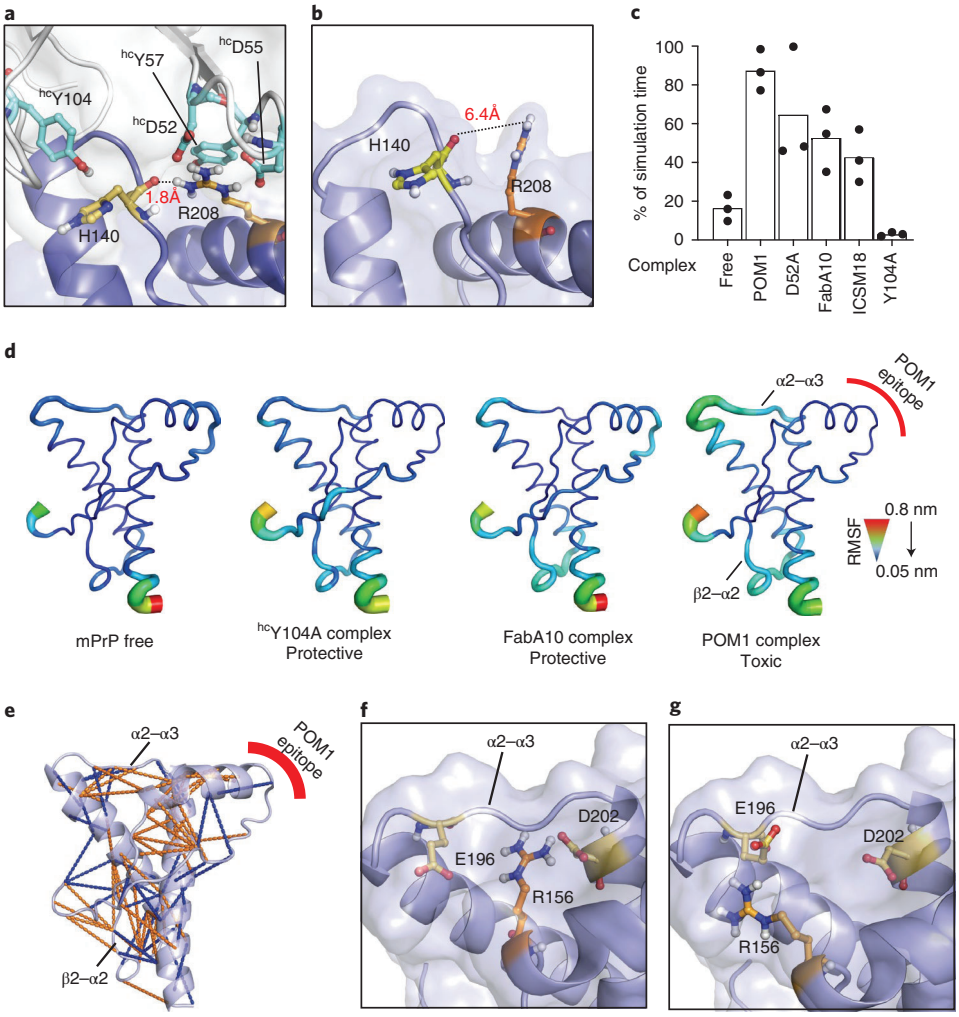

Fig. 1 | POM1 induces an intramolecular hydrogen bond between R208A and H140 of human PrP^C. a,**b**, Binding of PrP^C to the neurotoxic antibody POM1 favors the formation of a R208-H140 hydrogen bond in the GD of PrP^C (**a**) that is absent from free PrP^C (**b**). **c**, MD simulations indicate that toxic antibodies are more likely to induce the R208-H140 bond. Ordinate: percentage of simulation time in which the H-bond is present. See also Supplementary Figure 1. **d**, GD flexibility according to MD simulations. Narrow blue ribbons: rigidity; large green/red ribbons: increased flexibility. PrP bound to protective pomologs resembles free PrP. PrP bound to POM1 induces increased flexibility in the α2–α3 and β2–α2 loops. **e**, Binding of the toxic antibody POM1 to PrP induces local structural changes within the GD, here shown as a cartoon, both within and outside the epitope region. Side-chain contacts (less than 5 Å) that are present only in PrP free (blue, PDB 1xyx) or PrP bound (orange, PDB 4H88) are indicated by lines. **f**, POM1 binding breaks the R156-E196 interaction, increasing α2–α3 flexibility, and induces the formation of a R156-D202 salt bridge. **g**, R156 interacts with E196 in free PrP, which helps to rigidify the α2–α3 loop.

H-latch conformation (Fig. 3a–c). PrP^{2Cys} expressed in a *Prnp*$^{-/-}$ CAD5 cell line showed correct glycosylation and topology and did not trigger unfolded protein responses (Extended Data Fig. 3b,c). Surface-bound PrP^{2Cys} was detected by POM8 and POM19, which bind to a conformational epitope on the the α1–α2 and β1–α3 regions, respectively[7], but not by POM1 (Extended Data Fig. 2d,e). The POM1-induced H-latch allosterically altered the β2–α2 loop; similarly, binding of mPrP^{2Cys} to POM5 (recognizing the β2–α2 loop[7]) was impaired (Extended Data Fig. 2a). Taken together, these results suggest that mPrP^{2Cys} adopts a conformation similar to that induced by POM1 (Fig. 3c). We transduced *Prnp*$^{ZH3/ZH3}$ COCS with adeno-associated virus-based vectors (AAV) expressing either PrP^C or PrP^{2Cys}. Wild-type and mutant proteins showed similarly robust expression levels (Extended Data Fig. 3d). COCS expressing mPrP^{2Cys} developed spontaneous, dose-dependent neurodegeneration 4 weeks after transduction (Fig. 3d–f and Extended Data Fig. 3e,f), suggesting that induction of the H-latch is sufficient to generate toxicity. In agreement with this view, MD simulations showed that human, hereditary PrP mutations responsible for fatal prion diseases favor H-latch formation and altered flexibility in the α2–α3 and β2–α2 loops (Extended Data Fig. 4).

'Pomologs' rescue prion-induced neurodegeneration. If POM1 toxicity requires the H-latch, antibody mutants that are unable to induce it should be innocuous. POM1 immobilizes R208 by salt bridges with its heavy-chain (hc) residue ^{hc}D52, whereas ^{hc}Y104 contributes to the positioning of H140 (Fig. 1a). To prevent H-latch formation, we thus replaced eleven of these residues with alanine. For a control, we similarly substituted interface residues that are predicted to have no impact on R208. Resulting 'pomologs' were produced as single-chain variable fragments (scFv), three of which retained high affinity, that is a dissociation constant (K_D) of about 10 nM, for PrP^C (Table 1 and Extended Data Fig. 5).

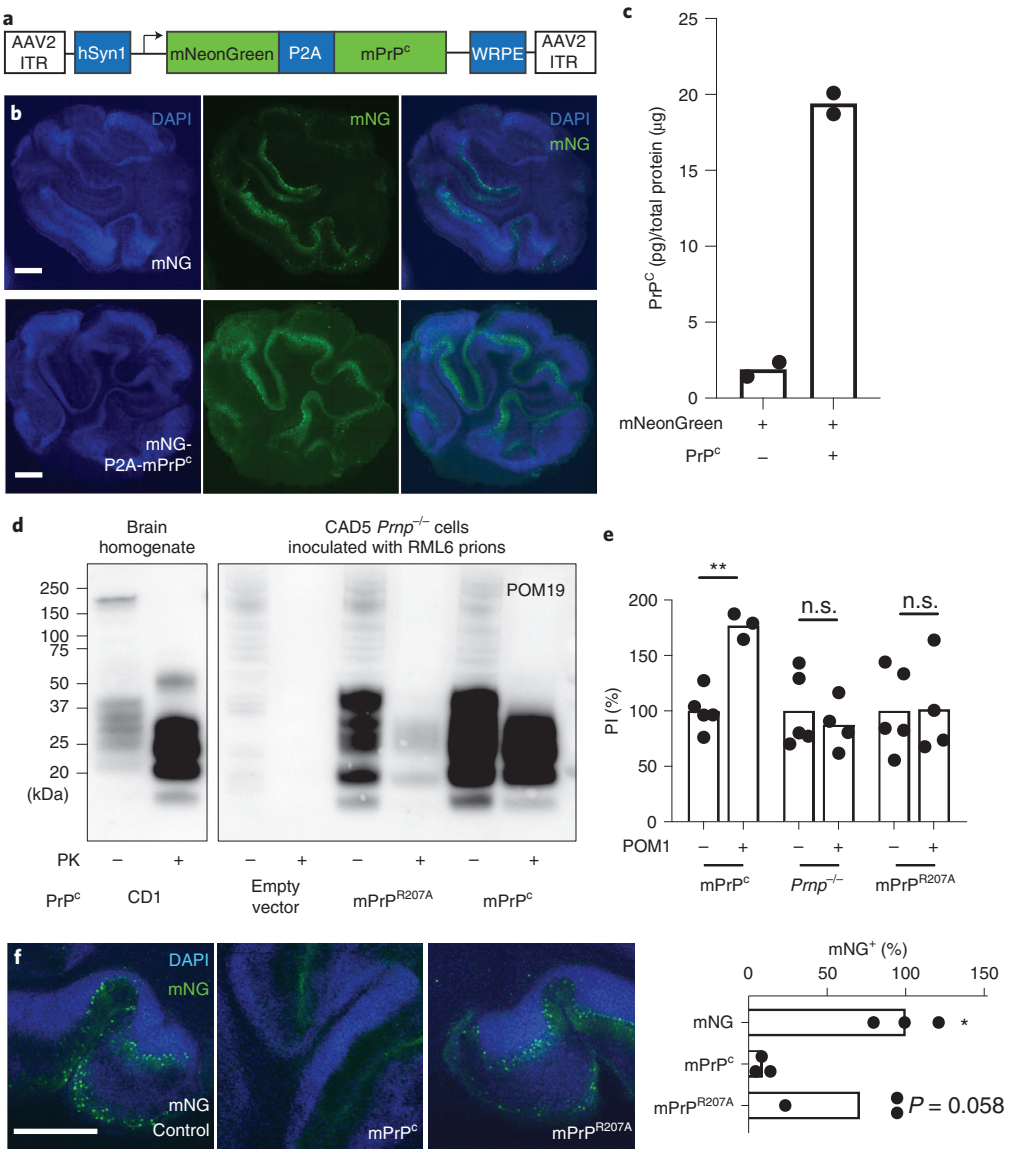

Fig. 2 | Ablation of H-latch formation by a R207A mutation in murine PrP^C rescues PrP-induced toxicity. a, Scheme of AAV used for bi-cistronic expression of monomeric NeonGreen and PrP^C, separated by a P2A site (monomeric neon green (mNG)-P2A-PrP^C). hSyn1, human Synapsin 1 promoter. WRPE, woodchuck hepatitis virus regulatory posttranscriptional element. ITR, inverted terminal repeats. **b**, Robust expression of mNG-P2A-PrP^C on fluorescent micrographs from transduced *Prnp*$^{ZH3/ZH3}$ COCS. Scale bars: 500 µm. **c**, Holo-POM19–holo-POM2-biotin PrP^C sandwich ELISA of samples depicted in **b**. One data point corresponds to a pool of 6–9 biological replicates of organotypic cultured slices. **d**, Proteinase K digestion of brain homogenates and cell lysates from chronically RML6-inoculated CAD5 cells (fourth passage is shown) detected with POM19. RML6 prions (lanes 1 and 2) and inoculated CAD5-mPrP^C cells (lanes 7 and 8) show a typical 'diagnostic shift' of proteinase K (PK)-digested PrP^{Sc}, whereas only trace amounts of PrP^{Sc} are detectable in CAD5-mPrP^{R207A} cells (lanes 5 and 6). Lack of detectable PrP^{Sc} in CAD5 *Prnp*$^{-/-}$ (lanes 3 and 4) cells indicates no residual inoculum. Lanes are from non-adjacent samples blotted on the same membrane. **e**, Addition of POM1 causes toxicity to CAD5 cells (left) but not to *Prnp*$^{-/-}$ or mPrP^{R207A} CAD5 cells (center and right). The percentage of propidium iodide (PI)-positive cells, determined by fluorescence-activated cell sorting (FACS), is shown on the *y* axis. Values are given as percentages of CAD5 mPrP^C PI-positive cells without POM1. One data point corresponds to a biologically independent cell lysate, for example a different cell passage. n.s., not significant, adjusted $P > 0.05$, **adjusted $P = 0.0083$, ordinary, one-way analysis of variance (ANOVA) with Šídák's multiple comparisons test. The FACS gating strategy is summarized in Extended Data Figure 3a. **f**, *Prnp*$^{ZH3/ZH3}$ COCS transduced with wild-type mPrP^C are susceptible to POM1 toxicity, whereas COCS transduced with control vector ('mNG control') or mPrP^{R207A} are not. Values are given as percentage of empty control. One data point corresponds to a biologically independent organotypic cultured slice. *adjusted $P = 0.012$, ordinary, one-way ANOVA with Šídák's multiple comparisons test. Scale bar: 500 µm.

As expected, all pomologs were innocuous to *Prnp*$^{ZH1/ZH1}$ COCS not expressing PrP^C (ref. [5]) (Extended Data Fig. 6a and Supplementary Fig. 1a). ^{hc}Y104A reduced H-latch formation, according to MD simulations (Fig. 1b and Supplementary Fig. 2) and exerted no neurotoxicity onto COCS from tga20 mice overexpressing PrP^C (ref. [16]), whereas POM1 and all H-latch inducing mutants (^{hc}D52A, ^{hc}Y101A and all light-chain pomologs) were neurotoxic (Fig. 4a and Extended Data Fig. 6b). As with POM1, the toxicity of pomologs required PrP^C, featured neuronal loss, astrogliosis and elevated levels of microglia markers (Extended Data Fig. 6c and Supplementary Fig. 1b), and was ablated by co-administration of the antibody POM2, which targets the flexible tail (FT) of PrP^C

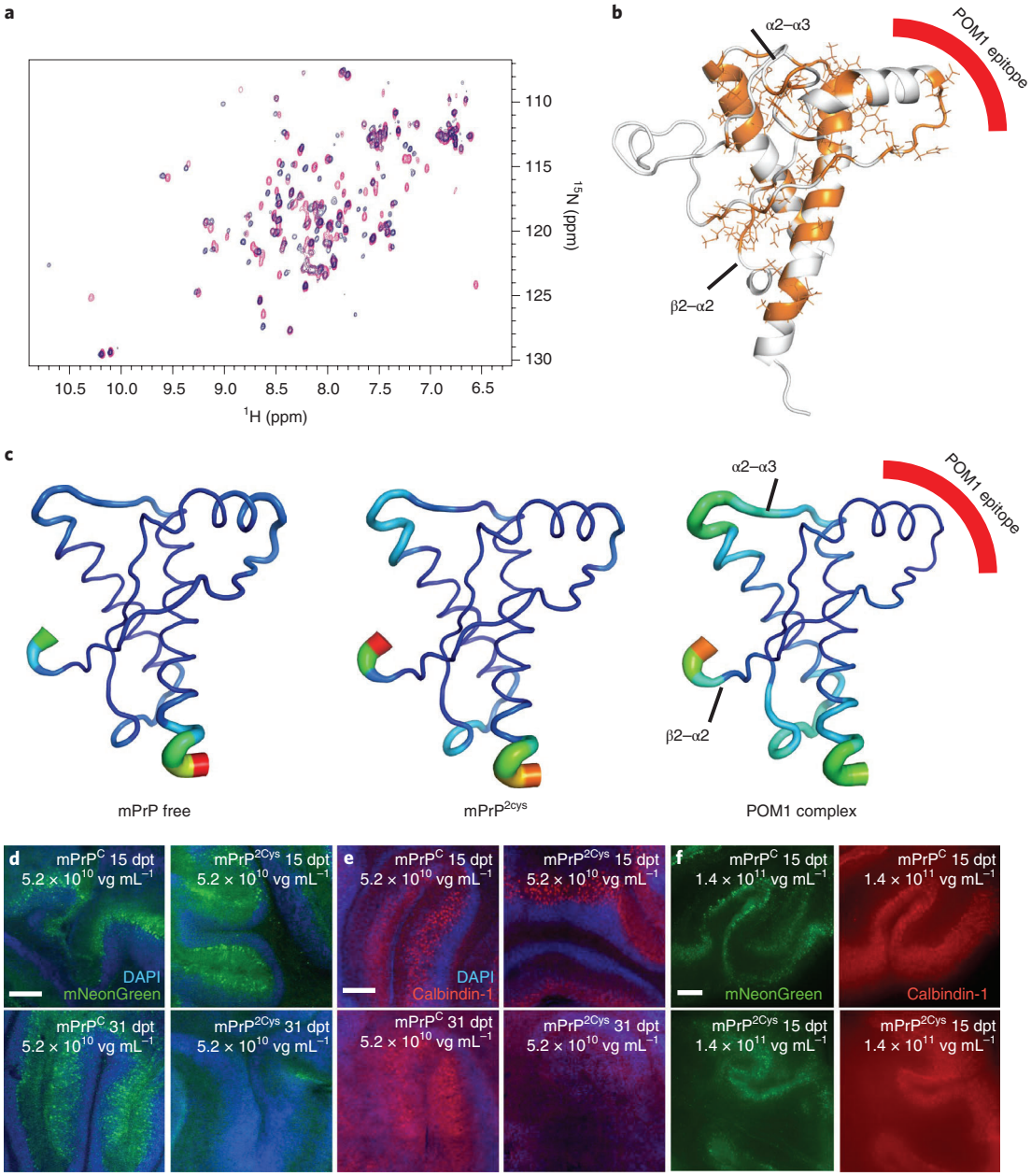

Fig. 3 | The R207C-I138C double-cysteine PrP^{C} mutant acts as an H-latch mimic. a,**b**, ^{15}N-heteronuclear single quantum coherence spectra of rmPrP free (red) and mPrP^{2cys} (blue). Residues with different chemical shifts in the two spectra are colored orange on the GD structure in **b**, which resemble the H-latch conformation in the POM1–PrP complex. **c**, MD simulations show that mPrP^{2cys} resembles the PrP–POM1 complex, with increased flexibility in the α2–α3 and β2–α2 loops and decreased flexibility in the 2Cys region, corresponding to the POM1 epitope. **d**–**f**, *Prnp*$^{ZH3/ZH3}$ COCS transduced with a bi-cistronic AAV expressing mNG and mPrP^{C} (left) or mPrP^{2Cys} (right). See Extended Data Figure 3f for quantification. Scale bars: 250 µm. **d**, mNG was visible in all COCS at 15 days post transduction (dpt, top row) but disappeared in mPrP^{2Cys} at 31 dpt (bottom row). **e**, Calbindin-1^{+} Purkinje cells were preserved at 15 dpt but became largely undetectable at 31 dpt, possibly as a result of mPrP^{2Cys} toxicity. **f**, Dose escalation of twice as many viral vectors as in **d** and **e** led to earlier onset of mPrP^{2cys}-mediated neurodegeneration. Significant neurodegeneration was observable at 15 dpt; see quantification in Extended Data Figure 3f.

(Extended Data Fig. 6d)[7]. Additionally, ^{hc}Y104A inhibited POM1 toxicity (Extended Data Fig. 6e,f).

POM1 does not induce de novo prions[10] but triggers similar neurotoxic cascades[8], plausibly by replicating the docking of prions to PrP^{C}. If so, ^{hc}Y104A may prevent the neurotoxicity of both POM1 and prions by competing for their interaction with PrP^{C}. Indeed, ^{hc}Y104A protected RML6 and 22L prion-inoculated tga20 and C57BL/6 COCS from prion neurodegeneration (Fig. 4b–d and Extended Data Fig. 6g–i), repressed the vacuolation of chronically prion-infected cells (Fig. 4e and ref. [2]) and diminished PrP^{Sc} levels ex vivo (Fig. 4f). In contrast to other antiprion antibodies[17], ^{hc}Y104A did not reduce levels of PrP^{C} (Fig. 4g), corroborating the conjecture that neuroprotection results from interfering with the docking of incoming prions.

The antibody ICSM18 was found to ameliorate prion toxicity in vivo[18], although dose-escalation studies have shown conspicuous neuronal loss[9]. The ICSM18 epitope is close to that of POM1 (ref. [12]), and MD simulations indicated that it facilitates the R208-H140 interaction, albeit less so than POM1 does (Fig. 1c).

Table 1 | a, Computational alanine scanning indicates which residues of POM1 and PrP contribute to binding. Positive numbers in the third column suggest loss of binding energy. b, On the basis of these results (Table 1a), we prepared 11 single mutations of POM1 (in each CDR loop) as scFv constructs. Colors (yellow to red) visualize the impact on binding affinity. The mutated residues are shown as sticks on the cartoon POM1 structure in Extended Data Figure 5b

A

Res N°	chain	ΔG(complex)	
32	L	0.44	POM1 residues
50	L	1.96	
91	L	2.09	
92	L	0.27	
93	L	0.28	
94	L	1.39	
96	L	0.35	
33	H	2.88	
52	H	2.47	
54	H	-0.02	
55	H	1.37	
57	H	1.76	
59	H	-0.01	
101	H	0.59	
103	H	-0.03	
104	H	4.91	
139	A	-0.01	PrP residues
146	A	-0.01	
138	A	0.11	
143	A	-0.21	
145	A	0.31	
141	A	0.39	
212	A	0.78	
140	A	0.93	
147	A	1.9	
144	A	3.44	
208	A	3.86	

B

	k_a (1/Ms)	k_d (1/s)	K_D (nM)	
POM1	6.4 x 10^4	3.1 x 10^-4	4.8	
hcW33A	no binding	no binding	no binding	CDR_H1 loop
hcD52A	3.3 x 10^5	4.6 x 10^-2	103	CDR_H2 loop
hcD55A	1 x 10^5	3.7 x 10^-2	372	
hcY57A	7.7 x 10^4	3.1 x 10^-2	406	
hcY101A	6.3 x 10^4	7.1 x 10^-4	11	CDR_H3 loop
hcY104A	3.6 x 10^4	2.1 x 10^-4	8.8	
lcS32A	6.4 x 10^4	5.9 x 10^-4	10	CDR_L1 loop
lcY50A	5.7 x 10^4	8.2 x 10^-3	313	CDR_L2 loop
lcS91A	1.3 x 10^4	1.8 x 10^-2	1430	CDR_L3 loop
lcW94A	3.1 x 10^5	2.7 x 10^-2	201	
lcY96A	6.2 x 10^4	7.4 x 10^-3	123	

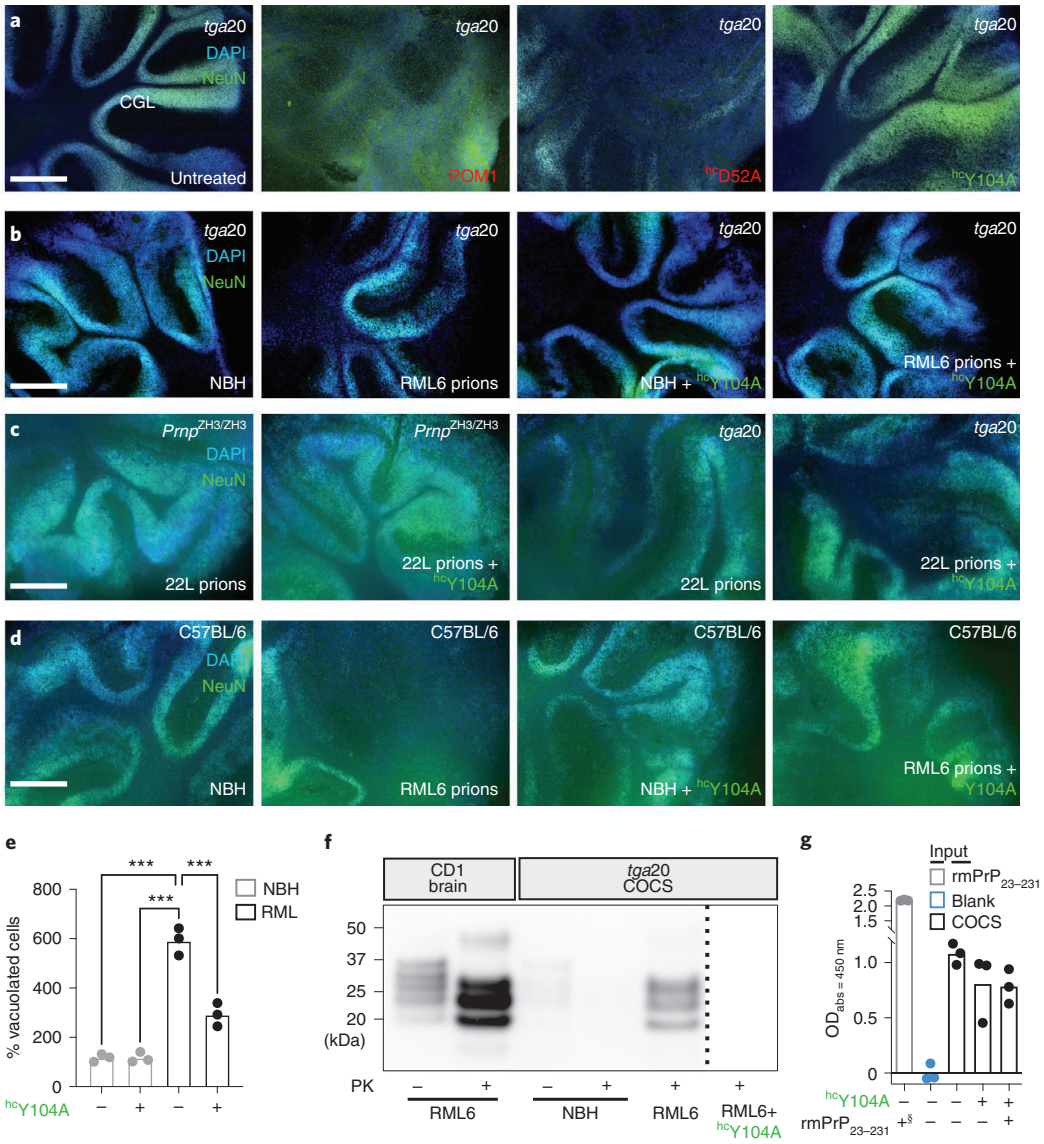

Fig. 4 | Preventing H-latch formation by pomologs rescues prion-induced neurodegeneration. a, The densely cellular NeuN^{+}DAPI^{+} cerebellar granule cell layer (CGL) of tga20 COCS was preserved by treatment with POM1 mutant ^{hc}Y104A (green) but destroyed by POM1 and ^{hc}D52A (red). **b**, CGL degeneration occurs in prion-infected tga20 COCS, but not in COCS exposed to non-infectious brain homogenate (NBH). Treatment of RML6 prion-infected tga20 COCS with ^{hc}Y104A prevented neuronal loss. **c**, Rescue of prion-induced toxicity by ^{hc}Y104A in COCS inoculated with 22L prions. **d**, Treatment of prion-infected wild-type COCS, expressing wild-type levels of PrP^{C}, with ^{hc}Y104A prevented CGL degeneration. **a**–**d**, Quantification of fluorescent micrographs is depicted in Extended Data Figure 6b,g–i. Scale bar: 500 µm. **e**, Treatment with ^{hc}Y104A (180 nM; 5 days) reduced vacuolation in chronically prion-infected Gt1 cells. Each dot represents an independent experiment with cells from different passages (1,000 cells/experiment, ordinary one-way ANOVA with Dunnett's multiple comparisons test, ****adjusted $P < 0.0001$). **f**, Treatment of prion-infected tga20 COCS with ^{hc}Y104A led to a reduction in PrP^{Sc} levels. One lane corresponds to a pool of 6–9 COCS digested with PK; PrP^{Sc} was detected using holo-POM1. The dashed bar indicates gel splicing of lanes running in non-adjacent wells on the same gel. **g**, Treatment of tga20 COCS with ^{hc}Y104A for 7 days did not reduce PrP^{C} levels, as determined by PrP^{C} sandwich ELISA. §870 pM of rmPrP$_{23230}$ were used as a positive control (first lane). Pomologs were pre-incubated with 600 nM of rmPrP$_{23-230}$ as negative controls (last lane). Ordinate: absorbance, given as optical density at $\lambda = 450$ nm.

Antibody binding causes conformational changes in GD and FT. Protective pomolog ^{hc}Y104A failed to induce the H-latch, which was induced by toxic mutations (Fig. 1c and Extended Data Fig. 1). MD simulations showed that POM1 rigidified its epitope but increased the flexibility of the α2–α3 and β2–α2 loops (Fig. 1c). Conversely, the conformation of PrP attached to the protective ^{hc}Y104A resembled that of free PrP. In accordance with MD simulations, NMR spectra, which are sensitive to local effects and transient populations[19], of rmPrP$_{90-231}$ in complex with POM1 revealed long-range alterations in the GD and in the adjacent FT (Fig. 5a). When bound to ^{hc}Y104A instead, rmPrP$_{90-231}$ elicited spectra similar to those of free PrP. Circular-dichroism (CD) spectroscopy showed that the full rmPrP (rmPrP$_{23-231}$)–POM1 complex had more irregular structure content than its free components (Fig. 5b), whereas no difference was observed when POM1 was complexed to partially FT-deficient rmPrP$_{90-231}$. We did not observe any changes in the secondary structure of the ^{hc}Y104A-bound rmPrP$_{23-231}$ complex. This suggests that POM1 can alter the FT conformation with two possible mechanisms. Either the secondary structure of the FT itself is changed, probably through a shift in the population of conformers (FT-changes), or the

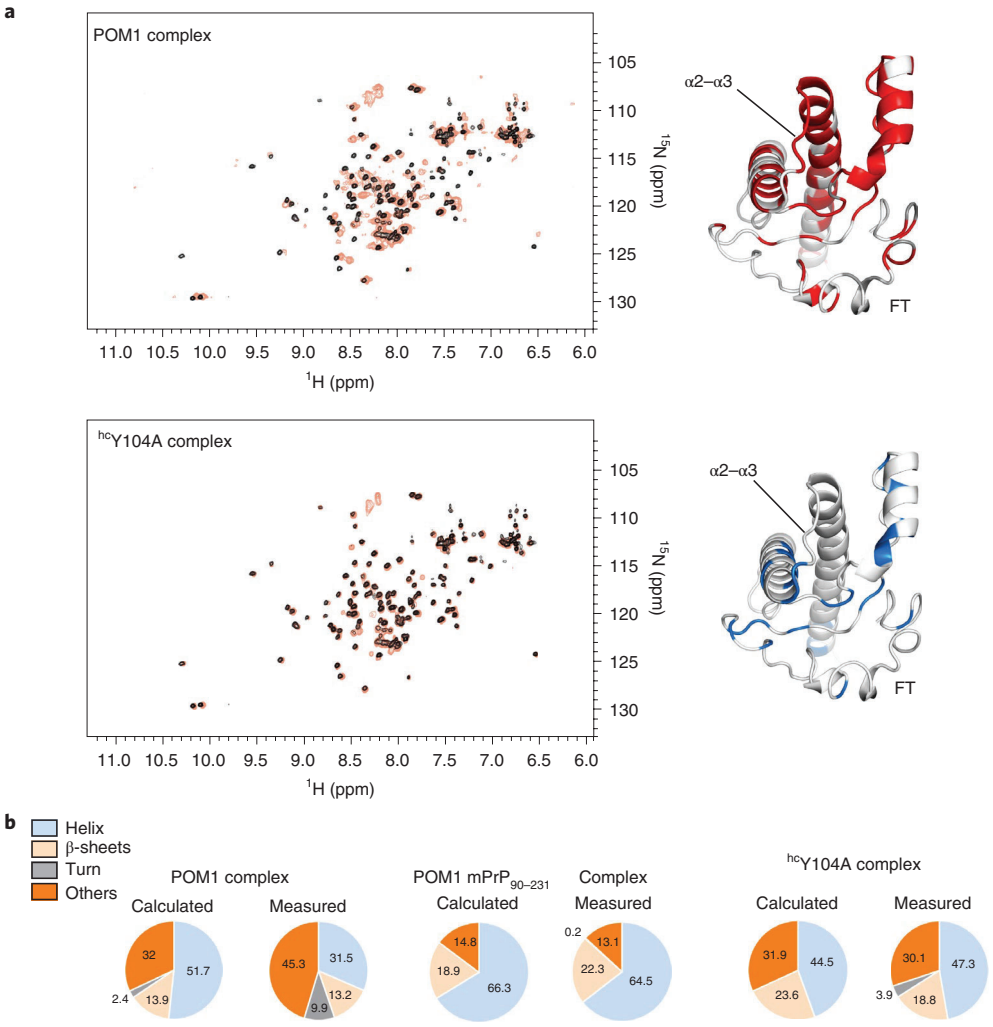

Fig. 5 | Antibody binding causes allosteric conformational changes in the GD and FT. a, Comparison between the [^{15}N,^{1}H]-TROSY spectra of free rmPrP$_{90–231}$ versus that bound to the ^{hc}Y104A pomolog. Chemical-shift differences, reflecting subtle alterations of the local chemical structure, were visible not only in the epitope but also at distant sites in the GD and FT. Residues affected by antibody binding are in color on PrP^{C} (GD and part of the FT are shown on a MD model of PrP). Differences between toxic and protective antibodies are evident in the α2–α3 loop (the Y104A complex is identical to free PrP^{C}) and in the FT region closer to the GD. **b**, Content of secondary structure estimated from CD spectra of the rmPrP–pomologs complexes. 'Calculated' indicates the secondary structure content if the rmPrP and pomolog did not change upon binding. POM1 displayed increased content of irregular structure (measured versus calculated) when in complex with full rmPrP$_{23–231}$, but identical content when in complex with a construct lacking the FT (rmPrP$_{90–231}$). This indicates that the FT changes conformation upon POM1 binding. Conversely, no differences were detected with the protective pomolog ^{hc}Y104A.

secondary structure of the GD is altered in a FT-dependent manner, with FT-GD interactions stimulated by POM1 binding. Hence H-latch induction leads to subtle alterations of the structure of both GD and FT, whose presence correlates with toxicity.

We performed animal experiments to confirm that (1) ^{hc}Y104A by itself is not neurotoxic in vivo, in contrast to POM1, and (2) it protects from prion-dependent neurodegeneration. When produced as IgG holoantibody, ^{hc}Y104A exhibited subnanomolar affinity to full-length, murine, recombinant PrP (rmPrP$_{23–231}$, Supplementary Fig. 2). We injected POM1 or holo-^{hc}Y104A into the hippocampus of C57BL/6 mice. Histology and volumetric-diffusion-weighted magnetic resonance imaging showed that POM1 (6 µg) elicited massive neurodegeneration that was repressed by pre-incubation with recPrP in threefold molar excess, whereas the same amount of holo-^{hc}Y104A did not elicit any tissue damage (Fig. 6a–g and Extended Data Figs. 7 and 8). A benchmark dose analysis[9] yielded an upper safe-dose limit of ≥12 µg for intracerebrally injected holo-^{hc}Y104A (Extended Data Fig. 8a). Also, the injection of holo-^{hc}Y104A (6 µg) into tga20 mice, which are highly sensitive to POM1 damage, failed to induce any lesions (Extended Data Fig. 8b–e).

We then transduced tga20 mice with ^{hc}Y104A by intravenous injection of a neurotropic AAV-PHP.B vector. Two weeks after AAV injection, mice were inoculated intracerebrally with 3×10^{5} ID$_{50}$ units of RML6 prions. ^{hc}Y104A expression levels correlated with both survival times and PrP^{Sc} deposition (Fig. 6h–j), suggesting that ^{hc}Y104A acts downstream of prion replication.

Phage displayed antibody fragments confer neuroprotection. If the same toxic PrP conformation is induced by both the H-latch and infectious prions, anti-PrP antibodies unable to bind the H-latch conformers could depopulate them by locking PrP^{C} in its innocuous state, thus preventing prion neurotoxicity. Using phage display (Extended Data Fig. 9a), we generated four antigen-binding fragments (Fabs), three of which bound the globular domain of PrP^{C} preferentially over PrP^{2Cys}, with one binding PrP and PrP^{2Cys} similarly (Fig. 7a and Extended Data Fig. 9b). When administered to

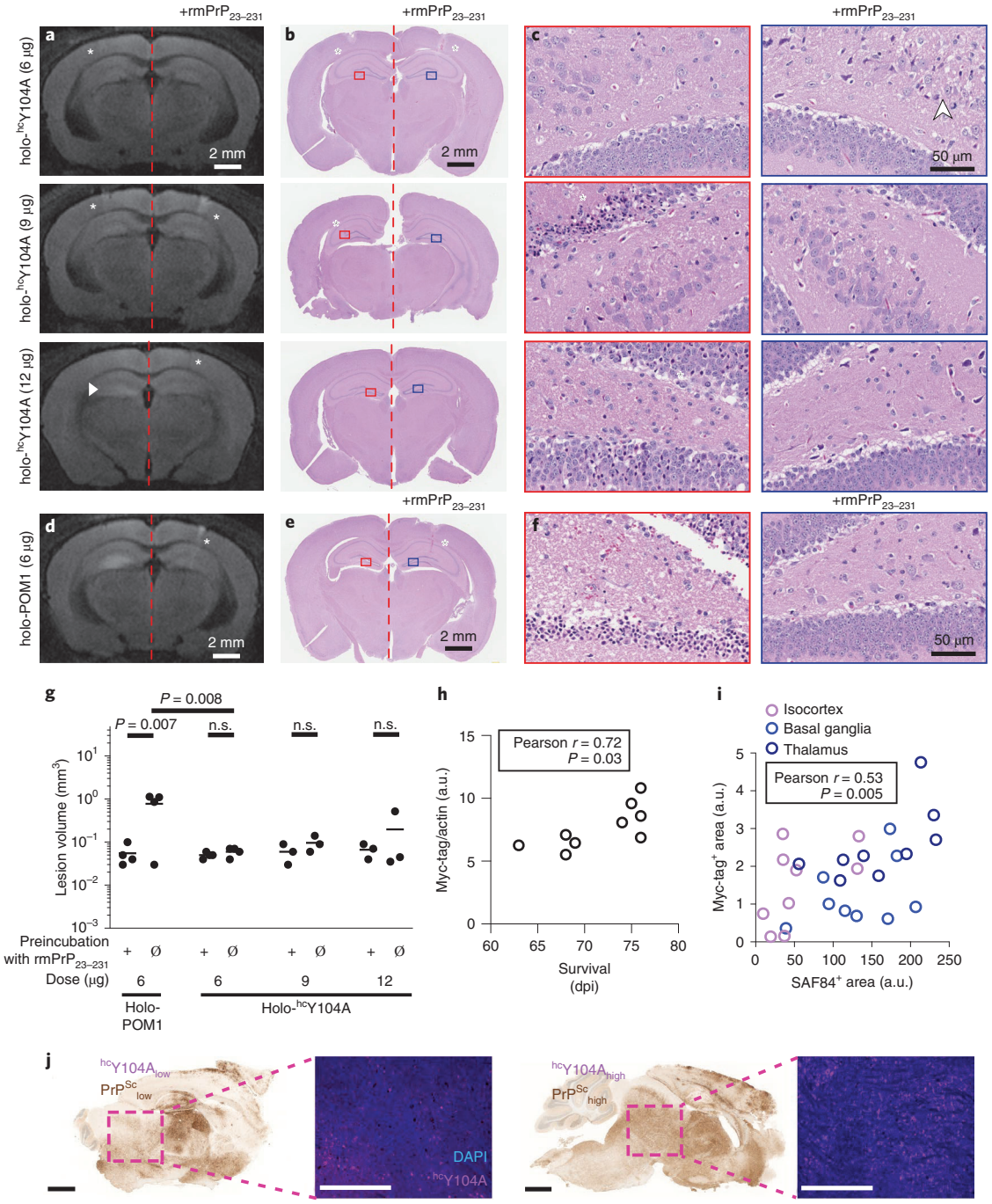

Fig. 6 | The holo-IgG antibody ^{hc}Y104A is innocuous after intracerebral injection. a, Representative magnetic resonance diffusion-weighted images (DWI) 24 hours after stereotactic injection of holo-^{hc}Y104A (left). Contralateral injections of holo-^{hc}Y104A + rmPrP$_{23231}$ (right). A small area of hyperintensity was found in one mouse after injection of 12 µg holo-^{hc}Y104A (white arrowhead). White asterisks: needle tract. **b**, Hematoxylin and eosin (HE)-stained sections from mice shown in **a**. Asterisks: needle tract. Rectangles denote regions magnified in **c**. **c**, HE sections (CA4). Left, holo-^{hc}Y104A injections (6, 9 and 12 µg). Right, holo-^{hc}Y104A + rmPrP$_{23-230}$. Asterisk (9 µg): neurons with hypereosinophilic cytoplasm and nuclear condensation in the vicinity of the needle tract. Asterisk (12 µg): These neurons were diffusely distributed among numerous healthy neurons. White arrowhead: vacuoles indicative of edema along the needle tract. **d**, DWI images of 6 µg holo-POM1 ± rmPrP$_{23-231}$, revealing a hyperintense signal at 24 hours. **e**, HE-stained section from a mouse shown in **d**. Asterisks: needle tract. Rectangles: areas in **f**. **f**, HE sections (CA4). Holo-POM1 injections revealed damaged neurons with condensed chromatin and hypereosinophilc cytoplasm. **g**, Volumetric quantification of lesions on DWI imaging 24 hours after injection revealed no significant lesion induction by holo-^{hc}Y104A. One datapoint corresponds to an animal. *P* values are adjusted for multiple comparisons. n.s.: not significant, $P > 0.05$, ordinary one-way ANOVA with Šídák's multiple comparisons test. **h**, Antibody expression levels, as determined by Myc-Tag western blot, showed a positive correlation with survival. One datapoint corresponds to one animal. Pearson correlation coefficient $r = 0.72$, 95% confidence interval 0.099–0.94, $P = 0.03$. a.u., arbitrary units. **i**, Significant correlation of PrP^{Sc} and antibody expression levels (representative images depicted in **j**, aggregated correlation across all brain regions). Different colors represent 3 brain regions from 9 independent animals. Pearson correlation coefficient $r = 0.53$, 95% confidence interval 0.18–0.76, $P = 0.0048$. **j**, Representative images from quantification of **I**. **I**, Sagittal brain sections stained with SAF84, highlighting PrP^{Sc}, and basal ganglia immunofluorescent micrographs marking ^{hc}Y104A-Myc-tag. Scale bar SAF84: 1 mm. Scale bar ^{hc}Y104A-Myc-tag: 500 µm.

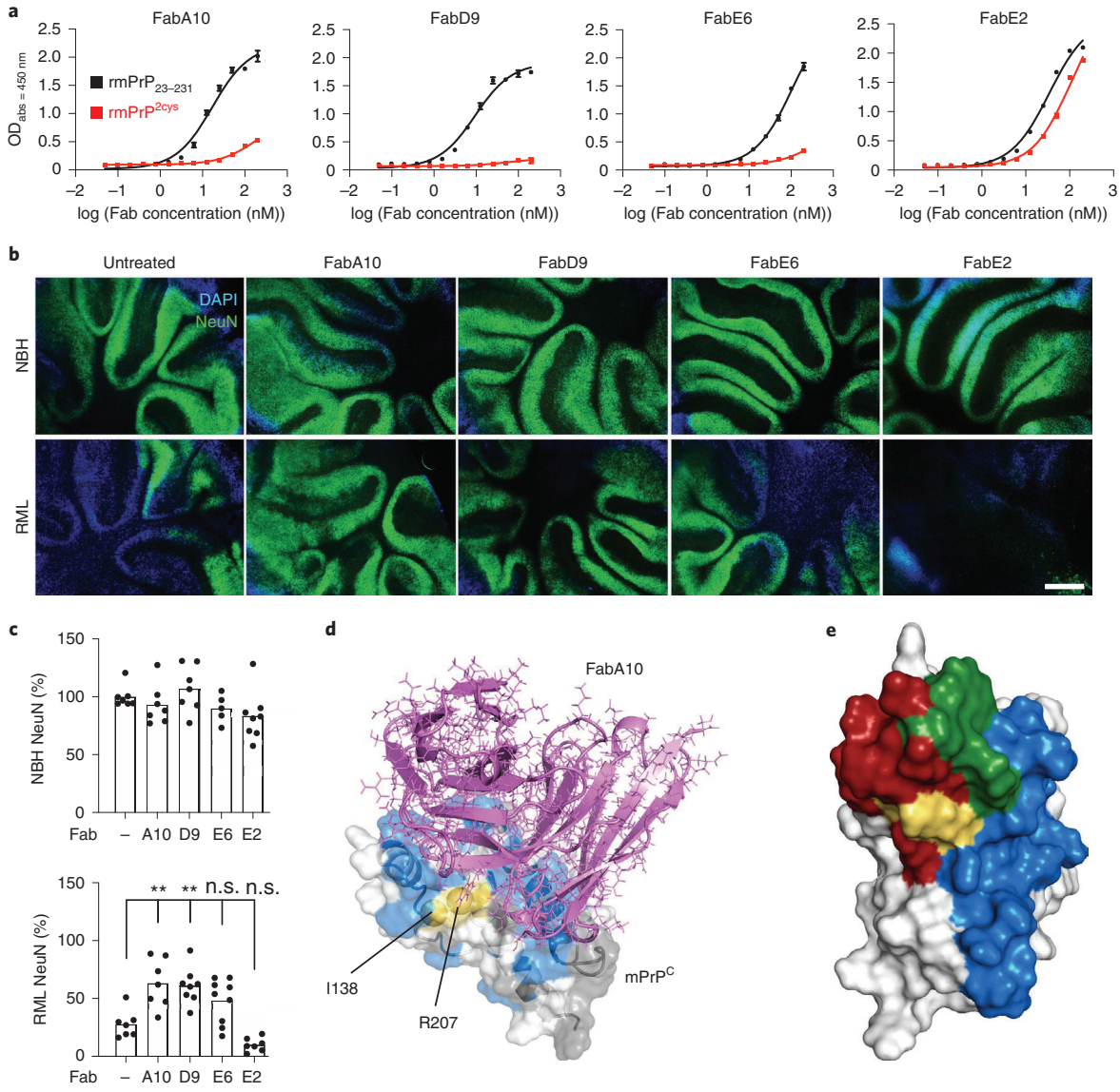

Fig. 7 | Phage-displayed antibody fragments differentially binding wild-type PrP^{C}, but not PrP^{2Cys}, confer neuroprotection. a, Preferential binding of the selected Fabs to rmPrP$_{23-231}$ over rmPrP^{2Cys}. With the exception of FabE2, the Fabs show higher apparent affinity for rmPrP$_{23-231}$ than rmPrP^{2Cys}. One datapoint corresponds to the mean ± s.e.m. of two technical replicates. The experiment was repeated twice. **b**, FabA10 and FabD9 conferred neuroprotection in prion-infected tga20 COCS. **c**, Quantification of NeuN fluorescence intensity from **b**, expressed as percentage of untreated (–) NBH. Scale bar: 500 µm. One datapoint corresponds to an independent, organotypic cultured slice. Two-way ANOVA with Dunnett's multiple comparison test, *P* values are adjusted for multiple testing: RML untreated (–) versus RML A10: $P = 0.006$, RML untreated (–) versus RML D9: $P = 0.009$, $^{**}P < 0.01$, n.s.: not significant, $P > 0.05$. **d**, Structure of PrP^{C} (white) in complex with FabA10 (violet) obtained by NMR-validated docking and MD. mPrP$_{90-231}$ residues whose NMR signal is affected by FabA10 binding are colored blue; residues with no NMR information are gray; residues mutated to Cys are yellow. **e**, There is partial overlap (green) between the epitopes of POM1 (red) and FabA10 (blue). The 2Cys are in yellow. PrP^{C} is depicted in different orientations in **d** and **e**.

prion-infected tga20 COCS, FabA10 and FabD9 decreased prion neurotoxicity, whereas FabE2, which binds both PrP^{C} and mPrP^{2Cys}, had no beneficial effect (Fig. 7b,c). NMR epitope mapping followed by computational docking and MD[20] showed that FabA10 binds to PrP encompassing the H-latch and partially overlapping with the POM1 epitope (Fig. 7d,e and Extended Data Fig. 10). MD showed that the H-latch is not stable in the presence of FabA10, even if the simulations were started from a POM1-bound PrP conformation with the R208-H140 H-bond present (Extended Data Fig. 10a).

Discussion

In summary, the evidence presented here suggests that H-latch formation is an important feature of prion toxicity. The H-latch was induced by the toxic anti-PrP antibody POM1, PrP mutants unable to form the H-latch conferred resistance to POM1 toxicity, and a PrP mutant mimicking the H-latch was constitutively neurotoxic. Conversely, POM1 mutants retaining their affinity and epitope specificity, but abolishing H-latch formation, proved to be neuroprotective. We observed that formation of the H-latch and its structural effects on PrP^{C}-GD were not only innocuous, but also protective against prion neurotoxicity in vitro and in vivo. The MD predictions were confirmed in vivo using both cerebellar slice cultures and mouse models of prion disease. POM1 mutants or other rationally selected Fabs that were unable to induce the H-latch protected from the deleterious effects of prion infection ex vivo and in vivo. Furthermore, hereditary PrP mutations leading to human prion